



## Two-qubit quantum gates with minimal pulse sequences

Ignacio R. Sola 

*Departamento de Química Física, Universidad Complutense, 28040 Madrid, Spain*

Seokmin Shin 

*School of Chemistry, Seoul National University, 08826 Seoul, Republic of Korea*

Bo Y. Chang \*

*School of Chemistry, Seoul National University, 08826 Seoul, Republic of Korea  
and Departamento de Química Física, Universidad Complutense, 28040 Madrid, Spain*



(Received 6 December 2023; accepted 19 April 2024; published 2 May 2024)

Working with trapped atoms at a close distance to each other, we show that one can implement entangling gates based on nonindependent qubits using a single pulse per qubit, or a single structured pulse. The optimal parameters depend on approximate solutions of Diophantine equations, causing the fidelity to never be exactly one, even under ideal conditions, although the errors can be made arbitrarily smaller at the cost of stronger fields. We fully characterize the mechanism by which the gates operate and study the effects of thermal motion and intensity fluctuations in the laser beams for different physical implementations of the gates. If instead of one pulse, we control the system with a two-pulse sequence, a plethora of mechanisms become possible where one can choose the optimal parameters from a wide range of values to achieve high-fidelity gates that are more protected from the effects of laser intensity fluctuations.

DOI: [10.1103/PhysRevA.109.052603](https://doi.org/10.1103/PhysRevA.109.052603)

### I. INTRODUCTION

Most quantum control protocols rely on complex pulse sequences or pulse structures in the time domain. We show in this work that, for ordered systems with a high degree of control in their spatial structure, it is possible to use the simplest pulse sequences and achieve the same level of control acting on the spatial degrees of freedom, adding some complexity in the spatial domain.

Quantum computers are the paramount systems where one needs a maximum degree of control over their spatial and time domain properties to minimize the effects of decoherence, and to synchronize the different interference effects that are involved in the speed-up properties of quantum algorithms [1–13]. Atoms trapped by optical tweezers [14–18], using highly excited Rydberg states for dipole-blockaded interactions [19–23], are one of the promising platforms for quantum computing due to their extended coherence times [13], strong and long-range interactions [13], scalability [14,24], and addressability [23,25–28]. This adaptability makes Rydberg atoms a versatile resource for implementing multiparticle entanglement [6,29–38], simple quantum circuits [27,33,39–51], and even quantum gates across different quantum computing platforms [52–57].

Current technology enables precise control over the position and spatial organization of the atoms in atomic traps, and this property has been extensively used for quantum

simulations and to prepare various entangled states [58,59]. Most quantum circuits, however, have relied on the use of independent qubits, which for homogeneous qubits impose large interatomic distances and hence operate with weak dipole blockades, leading to slow two-qubit gates. Several controlled-PHASE (CPHASE) [39,48,60] and controlled-NOT (CNOT) [40] gate proposals reported implementation times in the microsecond.

Since the ancillary states are highly excited (although long-lived) Rydberg states, speeding up the processes has obvious advantages, as it drastically reduces the effect of decoherence.

But this typically requires working with closer, and hence nonindependent, qubits, which brings an additional level of control in the atomic positions and the spatial profiles of the laser beams, for which we proposed a spatiotemporal control framework [61–63]. It turns out that by addressing both qubits at the same time using structured light and controlling the amplitude of the fields at the location of each qubit, one can extend the well-known scheme proposed by Jacksch *et al.* [39] with minimal changes, but working in the nanosecond regime, at least under ideal conditions [61]. The scheme, called the SOP (symmetrically orthogonal protocol), prepared a coherent dark state to transition the population through Rydberg states, isolating the effects of odd and even pulses in the pulse sequence, which added to the effect of the dipole blockade [61]. But by breaking the symmetry of the system with apparent disorder and fully controlling the spatial profile of the lasers, we showed that a multitude of schemes could implement the controlled-Z (CZ) gate with higher fidelity, in two-qubit [62] and  $N$ -qubit systems [63].

\*Corresponding author: boyoung@snu.ac.kr, bochang@ucm.es

Alternatively, there have been recent promising results addressing two or three qubits in symmetric arrangements of the atoms, which correspond to a very specific scenario from our setup of possible arrangements. Here, the control is enhanced by phase modulation of the pulses [51,64], so all the pulse complexity lies again in the time domain.

It is possible to classify the optimal control protocols obtained by numerical algorithms and to analyze the correlations among subsets of control parameters. In particular, we found highly constrained optimal parameters in protocols that use two-pulse sequences [62]. In this work, we focus on the minimal pulse sequences, where all the control practically depends only on the spatial domain. We find that, for nonindependent qubits, there are solutions that require a single pulse, which depends on approximate solutions of Diophantine equations. By scrutinizing the nature of two-pulse sequences, we determine the set of possible protocols and analyze the working principles behind their dynamics. In this work, we also propose a different physical realization of the nonindependent qubit gates, using partially superposed Gaussian beams, and provide an analysis of the role of the fluctuation and noise in the different control parameters on the robustness of the protocols.

## II. SETUP

### A. Dynamics

We study gate protocols based on nonindependent qubits that operate with pulses that interact with both qubits (or more than one qubit in the general setup) at the same time. Then, one must control both the temporal features of the pulse sequence (pulse areas, frequencies, relative phases) as well as the spatial properties of the pulse beams.

An example is the SOP scheme [61], where one applies a sequence of three structured pulses, using hybrid modes of light (e.g., superposition of TEM modes), with different amplitudes at the qubit sites:  $\Omega_k(\vec{r}_A, t) = a_k \mu_{0r} E_k(t)/\hbar = a_k \Omega_k(t)$ ,  $\Omega_k(\vec{r}_B, t) = b_k \mu_{0r} E_k(t)/\hbar = b_k \Omega_k(t)$ . The first pulse has a large amplitude on qubit A,  $a_1$ , and a smaller amplitude on qubit B,  $b_1$ . The second one reverts the role, but with a phase shift in one amplitude:  $a_2 = -b_1$ , and  $b_2 = a_1$ . Finally, the third pulse is a replica of the first one. The role of the  $a$  and  $b$  coefficients can be obviously interchanged. Arranging the factors that participate in the local amplitudes (hereafter called geometrical factors) as components of vectors  $\mathbf{e}_k$  (hereafter called structural vectors), we observe that  $\mathbf{e}_1 \mathbf{e}_2 = 0$  and  $\mathbf{e}_1 \mathbf{e}_3 = 1$ . The geometrical factors can be partially incorporated into the Franck-Condon factors  $\mu_{0r}$ , so one can assume, without loss of generality, that  $a_k$  and  $b_k$  are normalized to unity ( $|\mathbf{e}_k| = \sqrt{a_k^2 + b_k^2} = 1$ ).

For atoms a short distance apart, the dipole blockade forbids that more than one Rydberg state can be populated during the laser action. In the simplest model that describes the two-qubit gate [62], the system is described by eight states: the computational basis and ancillary states with Rydberg excitations, as the pulse frequencies are chosen to be in resonance with the  $|0\rangle \rightarrow |r\rangle$  transition [65]. The Hamiltonian is block-diagonal for each computational basis  $\mathbf{H}_k^V \oplus \mathbf{H}_k^A \oplus \mathbf{H}_k^B \oplus \mathbf{H}^D$ ,

where

$$\mathbf{H}_k^V = -\frac{1}{2}\Omega_k(t)(a_k|00\rangle\langle r0| + b_k|00\rangle\langle 0r| + \text{H.c.})$$

is the Hamiltonian of a three-level subsystem in  $V$  configuration, acting in the subspace of  $\{|00\rangle, |r0\rangle, |0r\rangle\}$  states, while  $\mathbf{H}_k^A = -\frac{1}{2}a_k\Omega_k(t)(|01\rangle\langle r1| + \text{H.c.})$  and  $\mathbf{H}_k^B = -\frac{1}{2}b_k\Omega_k(t)(|10\rangle\langle 1r| + \text{H.c.})$  are two-level Hamiltonians acting in the subspace of  $\{|01\rangle, |r1\rangle\}$  and  $\{|10\rangle, |1r\rangle\}$  respectively. We will refer generally to any of these subsystems with the superscript  $S$  ( $S = V, A, B$ ). Finally,  $\mathbf{H}^D = 0|11\rangle\langle 11|$  is the Hamiltonian acting on the double-excited qubit state  $|11\rangle$ , decoupled from any field.

Using temporally nonoverlapping pulses, the propagator for the time evolution is the time-ordered product of the evolution operators for each pulse,  $\mathbf{U}^S = \prod_{k=0}^{N_p-1} \mathbf{U}_{N_p-k}^S$ , which is analytical. For the  $V$  subsystem,

$$U_k^V = \begin{pmatrix} \cos \theta_k^V & ia_k \sin \theta_k^V & ib_k \sin \theta_k^V \\ ia_k \sin \theta_k^V & a_k^2 \cos \theta_k^V + b_k^2 & a_k b_k [\cos \theta_k^V - 1] \\ ib_k \sin \theta_k^V & a_k b_k [\cos \theta_k^V - 1] & b_k^2 \cos \theta_k^V + a_k^2 \end{pmatrix}, \quad (1)$$

where the mixing angle

$$\theta_k^V = \frac{1}{2} \int_{-\infty}^{\infty} \Omega_k(t) dt = \frac{1}{2} A_k$$

is half the pulse area. For the two-level subsystems A and B, we can use the same expression for the relevant states with  $a_k = 1, b_k = 0$ , for  $U_k^A$ , and vice versa for  $U_k^B$ . However, the mixing angles depend on the local coupling:  $\theta_k^A = a_k A_k/2$  and  $\theta_k^B = b_k A_k/2$ . We will refer to the generalized pulse areas,  $2\theta_k^S$ , as GPA.

The SOP uses spatially orthogonal vectors such that the state of the system after the first pulse acting on  $|00\rangle$  is a dark state of the Hamiltonian for the second pulse  $\mathbf{H}_2^V$ , so the second pulse does not affect this state. In this way, the SOP works similarly to the well-known protocol proposed by Jacksch and collaborators [39] (JP), but with nonindependent qubits. In this work, we will study families of schemes that can operate with even fewer pulses, although they typically require the same (or larger) accumulated pulse area,  $A_T = \sum_k |A_k|$ . In the following section, we propose a possible scheme to control the structural factors over a wide range of values (including negative factors) by using superposed laser beams.

### B. Implementation

Under the approximations of the effective Hamiltonian used in this work, the spatial control is encoded in the  $a_k$  and  $b_k$  parameters. In this section, we sketch several implementations that enable various degrees of control over the spatial features of the pulses. In Ref. [61] we proposed the use of hybrid modes of light to implement the SOP. Suppose that, for a certain step in the protocol, we want the laser  $k$  to act with spatial coefficient  $a_k$  at qubit A and  $b_k$  at qubit B, such as shown in Fig. 1(a). A suitable linear combination of electromagnetic modes  $\text{TEM}_{00}$  and  $\text{TEM}_{01}$ , centered at mid-distance between the qubits, can generate the pulse with the proper spatial values at the qubit sites. This implementation has the advantage of using a single pulse per step in the protocol.

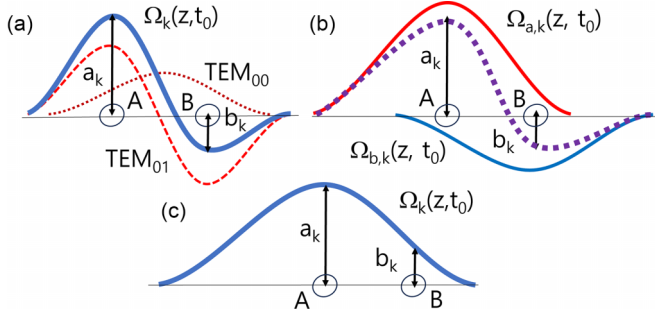


FIG. 1. Diagram showing the spatial profile of the pulses at  $t_0$  acting on the nonindependent qubits for different implementations of our scheme. In (a) the qubits are driven by a linear superposition of  $TEM_{00}$  and  $TEM_{01}$  modes of light, focused midway between the atoms, such that the amplitude of the field at qubits A and B is given by the desired controlled values,  $a_k$  and  $b_k$ . In (b) we achieve the same level of control by acting with two Gaussian beams focused on each atom. When the amplitudes  $a_k$  and  $b_k$ , and hence their ratio  $x_k$ , can be positive as in this work, it is possible to use a wide beam, centered on one qubit or in between, to achieve the desired control, as shown in (c).

However, it may require complex light structures [66–68] in systems with more than two qubits that could be too difficult to prepare in the laboratory. In addition, large values of  $a_k$  and  $b_k$  with opposite phases can put strong limits to the allowed spatial separation between the qubits.

In this work, we propose a different implementation based on partially superposed Gaussian beams [69,70] (although in principle, any beam shape is valid) centered at each atom. Assume again two qubits A and B at a distance  $R$  of each other, illuminated by pulses  $\Omega_{ak}$  (centered at qubit A), and  $\Omega_{bk}$  (centered at qubit B), as shown in Fig. 1(b). If both lasers have the same time dependence given by the function of time  $f(t)$ , at  $t_{0k}$  their sum will give the local field at  $\vec{r}_A$ ,  $\tilde{\Omega}_k(\vec{r}_A, t_{0k}) = \Omega_{ak}(\vec{r}_A, t_{0k}) + \Omega_{bk}(\vec{r}_A, t_{0k}) = [\tilde{\Omega}_{ak} + \sigma \tilde{\Omega}_{bk}] \equiv a_k \tilde{\Omega}_{0k}$ , where the Rabi frequencies with a tilde represent values at peak amplitude and  $\sigma = e^{-\alpha R^2}$  gives the overlap between the pulses, where  $\alpha$  is any measure of the beam's waist. We have assumed that the spatial profile of the lasers is the same for all the pulses in the sequence, as will be the case in most laboratory implementations. Correspondingly,  $\tilde{\Omega}_k(\vec{r}_B, t_{0k}) = \Omega_{ak}(\vec{r}_B, t_{0k}) + \Omega_{bk}(\vec{r}_B, t_{0k}) = [\sigma \tilde{\Omega}_{ak} + \tilde{\Omega}_{bk}] \equiv b_k \tilde{\Omega}_{0k}$ .

The geometrical factors  $a_k, b_k$  can be arranged as a column vector  $\vec{e}_k$ . In addition, we can define the column vector  $\tilde{\vec{e}}_k$  with components  $\tilde{\Omega}_{ak}, \tilde{\Omega}_{bk}$ , and the spatial overlap matrix

$$\mathbf{S} = \begin{pmatrix} 1 & \sigma \\ \sigma & 1 \end{pmatrix} \quad (2)$$

such that  $\tilde{\Omega}_{0k} \vec{e}_k = \mathbf{S} \tilde{\vec{e}}_k$  and  $\tilde{\vec{e}}_k = \tilde{\Omega}_{0k}^{-1} \mathbf{S}^{-1} \vec{e}_k$ ,

$$\begin{pmatrix} \tilde{\Omega}_{ak} \\ \tilde{\Omega}_{bk} \end{pmatrix} = \frac{\tilde{\Omega}_{0k}}{1 - \sigma^2} \begin{pmatrix} 1 & -\sigma \\ -\sigma & 1 \end{pmatrix} \begin{pmatrix} a_k \\ b_k \end{pmatrix}, \quad (3)$$

which gives

$$\frac{\tilde{\Omega}_{bk}}{\tilde{\Omega}_{ak}} = \frac{x_k - \sigma}{1 - \sigma x_k}, \quad (4)$$

where  $x_k = b_k/a_k$  is the ratio of the geometrical factors. For  $x_k \leq 1$ ,  $|\tilde{\Omega}_{bk}/\tilde{\Omega}_{ak}| < |b_k/a_k|$ . Whenever  $\sigma > x_k$ ,  $\tilde{\Omega}_{bk}/\tilde{\Omega}_{ak}$  must be negative. This can be achieved by controlling the relative phase between the pulses. In fact, one can use the superposition of Gaussian pulses as a technique to remove the effect of one pulse over an unwanted qubit, if we want to work with independent qubits even when  $\alpha \sim R^{-2}$ . In this case, the goal is to make  $\Omega_k(\vec{r}_b, t_{0k}) = 0$ , for which  $\tilde{\Omega}_{bk} = -\sigma \tilde{\Omega}_{ak}$ .

Using superposed Gaussian beams, it is always possible to control the geometrical factors of more than two qubits by controlling the ratio of the peak amplitudes of the fields (as well as the pulse phases). In the general case, one needs to define a different  $\sigma_{ab}$  for each pair of qubits. The matrix  $\mathbf{S}$  is always invertible, as long as  $\sigma_{ab} \neq 1$ , and thus two qubits do not occupy the same place.

Finally, for two-qubit or few-qubit systems, and positive relative ratios, it is possible to perform the operation with a single broad pulse, controlling the relative positions of the atoms with respect to the pulse waistbeam, as shown in Fig. 1(c). This again has the advantage of minimizing the number of pulses, reducing possible sources of error.

### III. SINGLE-PULSE PROTOCOLS

One of the advantages of working with nonindependent qubits is that it is possible to use shorter pulse sequences. In principle, there are enough control knobs to implement an entangling gate with a single-pulse sequence.

For the CZ gate, we use the unconventional (but equivalent) gate definition, where the amplitudes in each computational state, except the  $|11\rangle$ , experience a  $\pi$  shift at the end of the gate [39]. We calculate the fidelity as

$$F = \frac{1}{16} (-U_{11}^A - U_{11}^B - U_{11}^V + 1)^2, \quad (5)$$

where every term  $U_{11}^S$  is the first matrix element of Eq. (1). For each subsystem  $S$  of states coupled by the radiation, starting from the different computational states, one must then achieve  $\cos(\theta^S) = -1$ . These probability amplitudes correspond to so-called zero-loop processes [62], where the amplitude stays solely on the computational basis by the end of the pulse. For a single-pulse dynamics, only zero-loops can realize the gate. However, it is very simple to prove that zero-loops can never be exactly achieved for the three subsystems with a single pulse, so the gate mechanism cannot yield perfect fidelities even in the absence of noise or perturbations. The proof is simple to sketch.

Let the system have two qubits. For perfect fidelity, the following conditions must be satisfied:

$$\begin{aligned} \cos(A/2) &= -1 \rightarrow \sqrt{a^2 + b^2} A = (4l + 2)\pi, l \in \mathbb{Z} \\ \cos(aA/2) &= -1 \rightarrow aA = (4l' + 2)\pi, l' \in \mathbb{Z} \\ \cos(bA/2) &= -1 \rightarrow bA = (4l'' + 2)\pi, l'' \in \mathbb{Z}, \end{aligned} \quad (6)$$

where we used normalized structural factors. However, it is not possible to fulfill all the required conditions of Eq. (6) at the same time. Calling  $p = 4l + 2$ ,  $n = 4l' + 2$ ,  $m = 4l'' + 2$ , squaring the argument of the third condition, and comparing with the first two conditions, we obtain the relation between

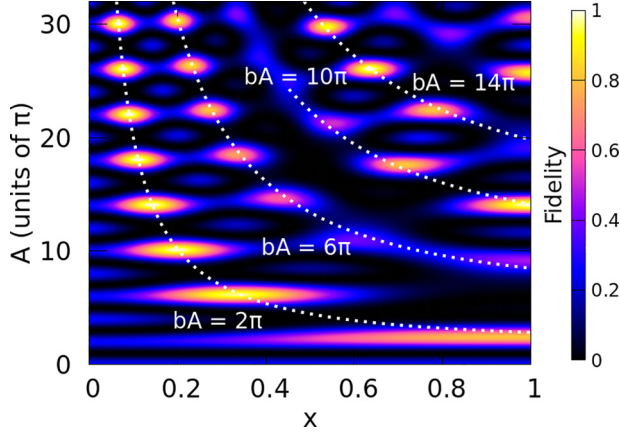


FIG. 2. Map of the fidelity for the CZ gate as a function of the pulse area and the ratio between the geometrical factors, for protocols based on a single pulse acting simultaneously on both qubits. In dashed lines, we show the protocols for which the action of the laser is minimal in the qubit  $b$ . The peaks appear at approximate solutions of a Diophantine equation.

the integers  $m, n, p$ :  $m^2 + n^2 = p^2$ . Equations like this that require integer solutions are generically called *Diophantine equations*. They have an infinite number of solutions, but it can be easily shown that the solutions cannot be constrained such that all  $m, n, p$  are of the form  $2, 6, 10, \dots, 4l + 2$ . For example, let  $p > n \geq m$ , such that  $m^2 = p^2 - n^2 = (p + n)(p - n) = 16(l + l' + 1)(l - l')$ . On the other hand, by directly squaring  $m^2$ , we obtain  $m^2 = 16(l'')^2 + 16l'' + 4$ . Both expressions must be equal. But, dividing both sides by 16, we have  $(l'')^2 + l'' + 0.25 = (l + l' + 1)(l - l')$ . The left-hand side cannot be integer, while the right-hand side is always integer.

It can be shown that the same restrictions apply whenever the logic tableaux implies an odd number of sign flips. For some nonentangling two-qubit phase gates, on the other hand, exact solutions may exist. This issue becomes more pronounced as the number of qubits increases. For instance, with three qubits, we have 3  $V$  subsystems and three two-level systems where the previous Diophantine approximate solutions must hold, in addition to a tripod system, which adds another equation like  $m^2 + n^2 + p^2 = q^2$ , that does not hold solutions for  $m, n, p, q$  integers of the type  $2, 6, \dots, 4l + 2$  or similar.

While it is not possible to achieve perfect fidelity, Eqs. (6) can be in principle fulfilled up to any desired accuracy. For instance, in the CZ gate,  $14^2 \approx 10^2 + 10^2$  with a relative error of approximately  $4/200 \approx 2\%$ , so that an approximate solution exists using equal geometrical factors in the qubits ( $a = b = 1/\sqrt{2}$ ) and a pulse area of  $A \sim 14\pi$ , which leads to a fidelity  $F = 0.992$ . In Fig. 2 we show a map of the fidelity of the gate as a function of the pulse area  $A$  and the ratio of the geometrical factors,  $x = b/a$ . Because the role of the geometrical factors is equivalent (the fidelity is the same for  $x$  and  $x^{-1}$ ), we only show the map for  $x \leq 1$ . The density of high-fidelity protocols increases for small  $x$  (or alternatively, for  $x \gg 1$ ). The simplest solutions involve  $bA = 2\pi$ . For large  $A$  and small  $b$ ,  $\sqrt{1 - b^2} \approx 1$  and  $aA \approx A$ . This gives the series

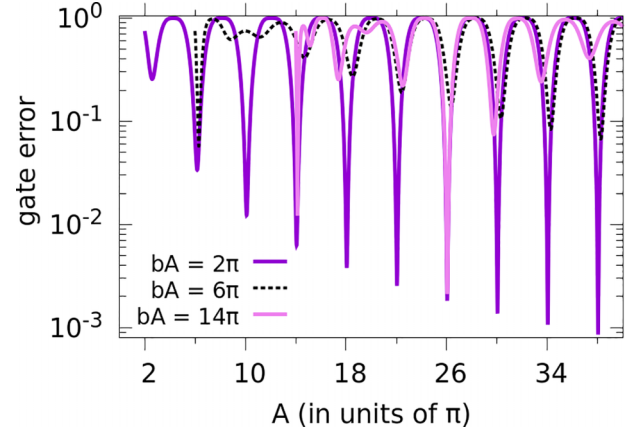


FIG. 3. Gate error as a function of the pulse area, for the solutions that satisfy  $bA = 2\pi, 6\pi, 14\pi$  (that is, for the set of points that follow the trajectory shown by the dotted lines in Fig. 2). In general, as  $bA$  increases, one needs larger areas to achieve high-fidelity protocols, but better approximate solutions of the Diophantine equations may exist for smaller areas, like  $A = 14\pi$  when  $a = b$ .

of solutions shown by the white dotted line in Fig. 2, where  $bA = 2\pi$ , from which

$$bA = \frac{x}{\sqrt{1+x^2}}A = 2\pi \rightarrow A = 2\pi \frac{\sqrt{1+x^2}}{x}. \quad (7)$$

A similar equation must be satisfied by  $aA$ . Dividing both, we obtain the values of  $x$  at which the fidelity is maximized,

$$x^{\text{op}} = \frac{b}{a} = \frac{bA}{aA} = \frac{4l'' + 2}{4l' + 2}. \quad (8)$$

For the smallest possible local area in qubit  $b$ ,  $bA = 2\pi$  ( $l'' = 0$ ),  $x^{\text{op}}$  lie in the sequence of inverse odd numbers,  $x^{\text{op}} = 1/(2l' + 1)$ . To fully optimize the gate, the contribution of the three terms  $U_{11}^A, U_{11}^B, U_{11}^V$  must be maximized, for which the optimal pulse area must be slightly corrected as the average between the value expected from Eq. (7) with  $x^{\text{op}}$ , and the value of the area that maximizes the  $U_{11}^V$  term,

$$A^{\text{op}} = (2l + 1 + \sqrt{(2l' + 1)^2 + (2l'' + 1)^2})\pi, \quad (9)$$

where  $l \geq l' \geq l'' \in \mathbb{Z}$ . The protocol with the smallest possible area ( $l, l', l'' = 0, 0, 0$ ) is achieved with  $A^{\text{op}} = 2.4\pi$  at  $x^{\text{op}} = 1$ , giving a relatively low fidelity of  $F = 0.804$ . The second maxima, at  $A = 6.17\pi$  with  $x = 1/3$ , gives already a fidelity  $F = 0.968$ . For very large integers, the relative error can be as small as desired by increasing the pulse area, properly adjusting the ratio of the geometrical factors following Eq. (8) and the area with Eq. (9). In Fig. 3 we show the gate error as a function of the pulse area, for protocols that obey  $bA = (4l'' + 2)\pi$  conditions. As expected, one needs larger areas to achieve high-fidelity protocols as  $bA$  increases, but better approximate solutions of the Diophantine equations may exist for smaller areas, as, e.g., when  $x = 1$  for  $A = 14\pi$ . However, as discussed in Sec. V, taking into account the effect of fluctuations in the parameters due to shot-to-shot noise can shift the maximum fidelities to the lower pulse area protocols.

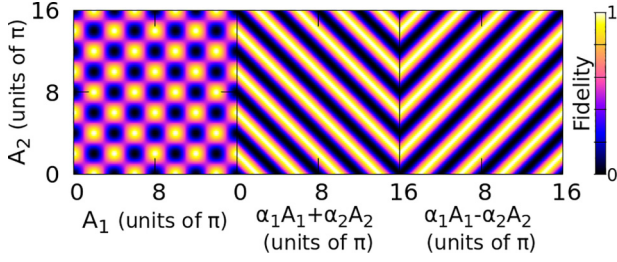


FIG. 4. The fidelity for protocols based on two-pulse sequences, as a function of the pulse areas, inherit the properties of  $-\cos(\theta_1) - \cos(\theta_2)$  (left) and  $-\cos(\theta_1 \pm \theta_2)$  (center and right). We represent the cosine scaled and shifted as  $(-\cos x + 1)/2$  so that its range is between 0 and 1, like the fidelity.

#### IV. TWO-PULSE PROTOCOLS

For two-pulse sequences, the time-evolution operators for the  $A$  and  $B$  subsystems have two terms,

$$U_{11}^{S'} = \cos(\alpha_2 A_2/2) \cos(\alpha_1 A_1/2) - \sin(\alpha_2 A_2/2) \sin(\alpha_1 A_1/2) \quad (10)$$

where  $S' = A, B$ ,  $\alpha = a, b$ , and the subscript refers to the pulse order. The first term is responsible for a gate mechanism based on a zero-loop, as in single-pulse sequences. The second term accounts for another mechanism that prepares the gate, the so-called one-loop, where the first pulse excites the population to the Rydberg state and the second pulse takes the population back to the computational basis [62]. For this to happen, the GPA must be an odd multiple of  $\pi$ . In the  $V$  subsystem, the second term is scaled by the product of the structural vectors,  $U_{11}^V = \cos(A_2/2) \cos(A_1/2) - \mathbf{e}_2 \mathbf{e}_1 \sin(A_2/2) \sin(A_1/2)$  ( $\mathbf{e}_2 \mathbf{e}_1 = a_1 a_2 + b_1 b_2$ ). For each subsystem, it is in principle possible to have gate mechanisms that behave as zero-loops, one-loops, or superpositions of both [62]. However, due to the  $\mathbf{e}_2 \mathbf{e}_1$  factor,  $U_{11}^V$  can only be close to  $-1$  if it follows a zero-loop or  $\mathbf{e}_2 \mathbf{e}_1 = \pm 1$ . In the latter case  $x_2$  must be equal to  $\pm x_1$ , forcing the structural vectors to be aligned or antialigned.

We will first analyze zero-loop protocols, which are a natural extension of single-pulse-based mechanisms. For zero-loop protocols in the  $V$  subsystem,  $\cos(A_2/2) \cos(A_1/2) = -1$ , which force  $A_1 = (4l + 2)\pi$  and  $A_2 = 4m\pi$  ( $l, m \in \mathbb{Z}$ ) or vice versa, forming the checkerboard pattern of the map of protocols as a function of the pulse areas (see Fig. 4 left), which was found by Sola *et al.* [62] using optimization algorithms.

In Fig. 5(a) we show the fidelity map as a function of  $A_2$  and  $x_2$ , after choosing  $A_1 = 6\pi$  and  $x_1 = 1/3$ , which are valid parameters in a single-pulse protocol. Hence,  $A_2 = 0$  is always a possible solution. In addition, all areas of the form  $A_2 = 4m$  ( $m \in \mathbb{Z}$ ) provide high-fidelity gates. As the choice of  $x_1$  forces the  $A$  and  $B$  subsystems to follow a zero-loop mechanism (since  $\cos \theta_1^{S'} = -1$ ,  $S' = A, B$ ), then  $a_2 A_2 = 4m'$ ,  $b_2 A_2 = 4m''$  and  $x_2^{\text{op}} = 4m''/4m'$ . Obvious solutions of the corresponding Diophantine equations show up at every  $m'$  for  $m'' = 0$  [since then  $m^2 = (m')^2$  exactly], but also, e.g., at  $m = 5$ ,  $m' = 4$ ,  $m'' = 3$ , for which  $x_2^{\text{op}} = 0.75$ , etc.

In Fig. 5(b) we choose  $A_1 = 4\pi$  and  $x_1 = 1/4$ . Solutions exist for all areas of the second pulse of the form  $A_2 =$

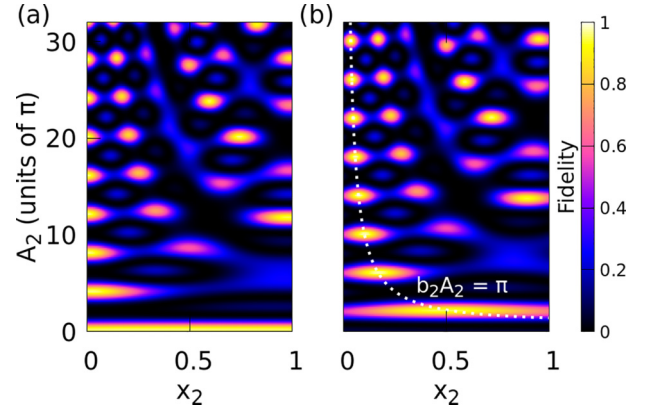


FIG. 5. Fidelity of the gate for two-pulse protocols as a function of  $x_2$  and  $A_2$ . In (a) we choose  $A_1 = 6\pi$  and  $x_1 = 1/3$ , which are parameters that prepare a high-fidelity gate in the absence of the second pulse, based on a zero-loop mechanism for all subsystems. In (b),  $A_1 = 4\pi$  and  $x_1 = 1/4$ , so that the gate follows a one-loop mechanism for the  $B$  subsystem. The maps are very similar to those of single-pulse sequences but with displaced areas and ratios of the geometrical factors.

$(4m + 2)\pi$ . Now,  $b_1 A_1 \approx \pi$ ,  $a_1 A_1 \approx 4\pi$ , so the first pulse opens a one-loop mechanism for the  $B$  subsystem, and a zero-loop mechanism for the  $A$  subsystem. Then, the sequence of fidelity peaks must occur at  $x_2^{\text{op}} = (2m'' + 1)/(4m' + 2)$  for all  $m', m'' \in \mathbb{Z}$ . For the smallest possible  $m'' = 0$ ,  $b_2 A_2 = x_2 A_2 / \sqrt{1 + x_2^2} \approx \pi$  and hence  $A_2 = \pi \sqrt{1 + x_2^2}/x_2$ . This is the dotted line shown in Fig. 5(b) for which high-fidelity peaks show up at  $x_2^{\text{op}} = 1/2, 1/6, 1/10, \dots, 1/(4m' + 2)$ .

It is important to note, however, that any superposition of mechanisms can occur in the  $A$  and  $B$  subsystems. As long as the pulse areas  $A_1$  and  $A_2$  alternate as  $(4l + 2)\pi$  and  $4m\pi$  or vice versa, it is always possible to find high-fidelity protocols for any  $x_1$ , because from Eq. (10),  $U_{11}^{S'} = \cos(\theta_2 \pm \theta_1)$ , with  $\theta_k = \alpha_k A_k/2$  ( $\alpha = a, b$ ). The minus sign inside the cosine applies when the ratios ( $x_1$  and  $x_2$ ) or areas ( $A_1$  and  $A_2$ ) change signs. There will always be values of  $x_1, x_2$  (or, more precisely, of  $a_1 A_1 + a_2 A_2$  and  $b_1 A_1 + b_2 A_2$ ) for which  $U_{11}^{S'} = -1$  for the choice of pulse areas  $A_1, A_2$  that make  $U_{11}^V = -1$ . Depending on  $x_1$  and  $x_2$ , the  $A$  and  $B$  subsystems belong to a continuous range of mechanisms, from zero-loops to one-loops, passing through any combination.

Can this realization of every possible mechanism include the  $V$  subsystem? Indeed, if the structural vectors are aligned or antialigned,  $\mathbf{e}_1 = \pm \mathbf{e}_2$ , for which  $x_2 = \pm x_1$ , then the three terms  $U_{11}^S$  ( $S = A, B, V$ ) behave as Eq. (10), which can be written as  $\cos(\theta^S)$ , with  $\theta^V = (A_1 \pm A_2)/2$ ,  $\theta^{S'} = (\alpha_1 A_1 + \alpha_2 A_2)/2$  ( $S' = A, B$ ). These are exactly the same equations as in the single-pulse sequence, except that now the argument depends on the sum of pulse areas,

$$A_T = A_1 \pm A_2 = (4n + 2)\pi, \quad n \in \mathbb{Z}, \quad (11)$$

where the plus sign applies for aligned vectors and the minus for antialigned vectors. So, every combination of pulse areas that sums  $(4n + 2)\pi$  can generate a high-fidelity gate, where the mechanism can be any superposition of zero-loops and one-loops for all the different subsystems.

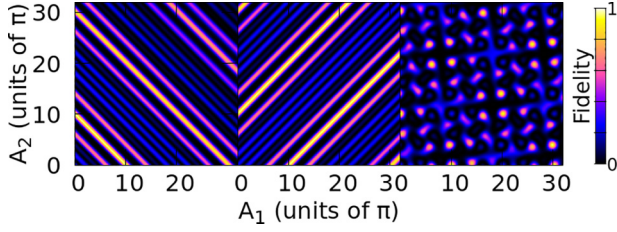


FIG. 6. Fidelity map as a function of the pulse areas  $A_1$  and  $A_2$  for (left) aligned structural vectors with  $x_1 = x_2 = 1/5$ , (center) antialigned structural vectors with  $x_1 = -x_2 = 1/5$ , and (right) orthogonal structural vectors with  $x_1 = -1/x_2 = 1/5$ .

In Fig. 6 we show the fidelity map as a function of the pulse areas  $A_1$  and  $A_2$  for  $x = x_1 = x_2 = 1/5$  (left) and  $x = x_1 = -x_2 = 1/5$  (center). There are high-fidelity straps for pulse areas that sum  $(4n + 2)\pi$ , but not for all values of  $n$ . The actual maximum fidelity observed and its location depends on the choice of  $x$ . The direction of the straps depends on whether the vectors are aligned or antialigned. These patterns inherit the properties of  $-\cos(\theta_1 \pm \theta_2)$  shown in Fig. 4. In Fig. 7 we show the fidelity map as a function of  $x$  and  $A_2$ , where we fixed  $A_1 = 7\pi$  for both aligned (a) and antialigned (b) vectors. As observed,  $A_2 = (4n - 5)\pi$ .  $x = x_2 = x_1$  [Fig. 7(a)],  $x = x_2 = -x_1$  [Fig. 7(b)]. The solution that appears at  $x = 0.2$  corresponds to  $A_2 = 3\pi$  (the sum of areas equals  $10\pi$ ). Allowing  $x$  to change, one can typically find high-fidelity protocols for any possible valid  $n$ , and consequently, for any  $A_2$  [71].

Finally, it is even possible to find optimal protocols where the structural vectors are orthogonal,  $\mathbf{e}_1 \mathbf{e}_2 = 0$ . They imply a superposition of the aligned and antialigned vectors, for which the fidelity map looks like the pattern observed in Fig. 6 (right). The fidelity peaks now form a rotated lattice. The peaks are a distance of  $4\pi$  apart, and the angle of the lattice depends on the choice of  $x$ . These are the solutions explored in the so-called SOP (symmetrical orthogonal protocol), explained in Ref. [61].

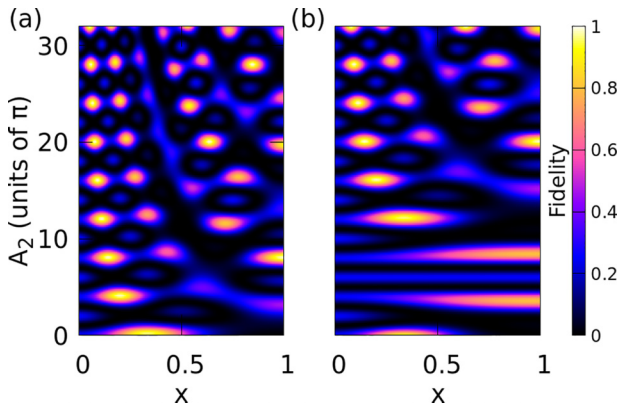


FIG. 7. Fidelity map as a function of the second pulse area  $A_2$  and the ratio of geometrical factors  $x$  for (a) aligned ( $x_2 = x_1$ ) and (b) antialigned ( $x_2 = -x_1$ ) structural vectors. For the figure, we choose  $A_1 = 7\pi$ .

## V. EVALUATING THE EFFECTS OF NOISE

To analyze in detail all the effects of noise on the proposed schemes, one needs to better define the setup of the system, choosing very concrete parameters for the lasers and atomic traps, which is outside the scope of this work. Our analytical approach follows from an approximate Hamiltonian from which we can obtain the time-evolution operator, so we cannot incorporate the sources of noise at the level of the dynamical description. From the physical point of view, the schemes shown here operate using the Rydberg blockade, so one can expect a similar sensitivity to the fluctuation of the laser frequency, the spontaneous emission, and the thermal motion of the atoms, as reported elsewhere [72]. However, because the atoms are much closer, the dipole blockade much larger, and the pulses much shorter (operating, in principle, in tens of nanoseconds) and much more intense, the phase-induced detunings or changes in population due to spontaneous decays—which are the main sources of errors in microsecond experiments—become almost negligible in our setup. Mainly shot-to-shot fluctuations, rather than decoherence, will have some impact on the fidelities.

Herein, we develop a simple model to evaluate the impact of fluctuations in the pulse energy (hence pulse areas) and geometrical factors on the fidelity for the CZ gate in two-qubit systems, using two partially overlapping pulse beams centered at each qubit.

The impact of amplitude fluctuations over the pulse areas is direct. For a pulse with intensity  $I_0 \propto \tilde{\Omega}_0^2$ , given that the area is  $A_0 = \tilde{\Omega}_0 S_0 / \hbar$ , where  $S_0$  is a shape factor, neglecting fluctuations in the pulse duration (or rather, subsuming the effect on the peak intensity fluctuation), the relative error in the pulse areas is

$$\delta A_0 \equiv \Delta A_0 / A_0 = \Delta I_0 / 2I_0. \quad (12)$$

Using stabilized microsecond pulses,  $\delta I_0$  can be estimated as  $\sim 3\%$  or smaller [72].

Fluctuations in the geometrical factors depend both on fluctuations in the laser amplitudes as well as on the thermal motion of the atoms. For  $x_k$  obtained by a superposition of beams,

$$x_k = \frac{\tilde{\Omega}_{bk} + \sigma \tilde{\Omega}_{ak}}{\tilde{\Omega}_{ak} + \sigma \tilde{\Omega}_{bk}}, \quad (13)$$

we estimate, for the fluctuation on the intensity of the pulses,

$$\left( \frac{\partial x_k}{\partial \tilde{\Omega}_{ak}} \right)^2 (\Delta \tilde{\Omega}_{ak})^2 = \left( \frac{\sigma - x_k}{\tilde{\Omega}_{ak} + \sigma \tilde{\Omega}_{bk}} \right)^2 \left( \tilde{\Omega}_{ak} \frac{\delta I_0}{2} \right)^2 \quad (14)$$

$$\left( \frac{\partial x_k}{\partial \tilde{\Omega}_{bk}} \right)^2 (\Delta \tilde{\Omega}_{bk})^2 = \left( \frac{1 - \sigma x_k}{\tilde{\Omega}_{ak} + \sigma \tilde{\Omega}_{bk}} \right)^2 \left( \tilde{\Omega}_{bk} \frac{\delta I_0}{2} \right)^2. \quad (15)$$

Since  $(\sigma - x_k)^2 \tilde{\Omega}_{ak}^2 = (1 - \sigma x_k)^2 \tilde{\Omega}_{ak}^2$  by Eq. (4), summing both terms, we obtain an error of the order of  $x^2 (\delta I_0)^2 / 2$  (actually, strictly smaller than this value, for positive  $x_k$ ).

For the fluctuation in the atomic positions due to thermal motion, assuming pulse beams overlap such that  $2\alpha R^2 \sim 1$ ,

we obtain

$$\left(\frac{\partial x_k}{\partial \sigma}\right)^2 \left(\frac{\partial \sigma}{\partial R}\right)^2 (\Delta R)^2 = \left(1 - \frac{\tilde{\Omega}_{bk}(\sigma + x_k)}{\tilde{\Omega}_{ak} + \sigma \tilde{\Omega}_{bk}}\right)^2 (\sigma \Delta R)^2, \quad (16)$$

which is of the order of (and for positive  $x_k$ , strictly smaller than)  $(\sigma \Delta R)^2$ . Assuming independent sources of fluctuation, the overall error can be written as

$$(\delta x_k)^2 = \frac{1}{2}(\delta I_0)^2 + \frac{\sigma^2}{x_k^2}(\delta R)^2. \quad (17)$$

To evaluate the error in  $\delta R$ , we use a simple estimation assuming a diffusion model for the dispersion of the atoms,  $\Delta R \sim \sqrt{2Dt_g}$ , where  $t_g$  is the gate duration and  $D$  the diffusion coefficient. In Ref. [72], working with atoms separated  $5\mu\text{m}$  and using gates that operate in  $\sim 5\mu\text{s}$  at  $\sim 25\mu\text{K}$ , the authors evaluate  $\Delta R$  as  $\sim 50\text{nm}$ . If we assume that our gates operate under similar conditions (e.g., temperature) but 25 times faster, that would imply  $\Delta R \sim 10\text{nm}$ , for a relative error of  $\delta R \sim 1\%$  when the atoms are approximately  $1\mu\text{m}$  apart, although our approximations may underestimate the error during the measuring of the gate's state. To evaluate the effect of the temperature, we will assume a linear dependence with the mean square displacement, as in Brownian motion, or for classical and quantum oscillators under certain limits [73,74].

We use Eqs. (12) and (17) to evaluate a distribution of parameters  $A$  and  $x$  following the noise statistics. We also include a Gaussian distribution in the absolute phase of the lasers with standard deviation  $\Delta\phi$ . Mean fidelities  $\bar{F}$  and standard deviations  $\delta F$  are obtained after analyzing the results with 1000 samples of the noisy parameters for several single-pulse optimal protocols (with  $l'' = 0$  and  $l = l'$ ) with different noise contributions. In Fig. 8 we show the fidelities in the absence of fluctuations (circles) and the average fidelities with  $\delta I = 0.03$ ,  $\delta R = 0.01$  ( $T \sim 25\mu\text{K}$ ) and  $\Delta\phi = 0.1\pi$ , labeled as “standard,” which are the errors reported in Ref. [72]. The error bars  $\delta F$  show how much the fidelity fluctuates for different experiments, reaching  $\delta F = 0.17$  for  $l' = 6$ . The results reveal that the fidelity is severely affected for protocols with large  $l'$  (and  $l$  and hence  $A$ ), which correlates to protocols that operate with larger Rabi frequencies and smaller ratios of the geometrical factors.

The effect of fluctuations in the laser amplitudes (purple lines) is significantly stronger than the effect of fluctuations on the atomic positions due to the thermal motion of the atoms (gray lines). Although the relative error in both  $A$  and  $x$  is linearly proportional to the relative error in the pulse intensities, the required precision in the intensities should increase for protocols that use stronger fields, as a small error in  $A$  can easily shift the GPA from an odd multiple to an even multiple of  $\pi$  (and vice versa), completely changing the excitation mechanism. Hence, for intensity fluctuations of  $\sim 3\%$ , only the lowest area protocols ( $A \leq 10\pi$ ) survive with fidelity errors smaller than 5%. It is necessary to reduce the laser fluctuations to one-half of this value or lower (1.5% in solid purple line) to reduce the gate errors to less than 2% in protocols with  $A = 14\pi$ . For comparison, to observe the same level of error from thermal effects only, we need to increase

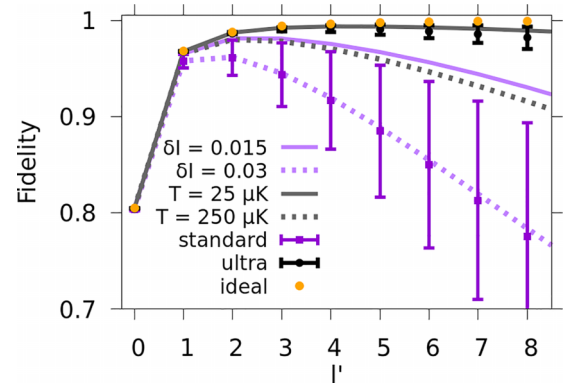


FIG. 8. Fidelity for single-pulse protocols with different  $l = l'$  and  $l'' = 0$  for different levels of noise in the parameters. Gray lines show the mean fidelities when the noise is induced by thermal fluctuations in the positions of the atoms, with relative standard deviations  $\delta R = 0.0316$ , corresponding to  $T = 250\mu\text{K}$  (dotted), and  $\delta R = 0.01$ , corresponding to  $T = 25\mu\text{K}$  (solid). Purple lines show the mean fidelities when the noise is induced by fluctuations in the peak intensities of the pulse, with relative standard deviations  $\delta I = 0.03$  (dotted) and  $\delta I = 0.015$  (solid). Lines with error bars show the mean and standard deviations for the results in the presence of both noise sources, in different laboratory conditions that we termed “standard” ( $T = 25\mu\text{K}$ ,  $\delta I = 0.03$ ,  $\Delta\phi = 0.1\pi$ , in dark violet) and “ultra” ( $T = 3\mu\text{K}$ ,  $\delta I = 0.007$ ,  $\Delta\phi = 0.01\pi$ , in black). Finally, the circles are the results in ideal conditions.

the temperature by a factor of 10, as shown in the dotted gray line ( $T \sim 250\mu\text{K}$ ,  $\delta R \sim 0.032$ ).

In Fig. 8, labeled as ultra, we show also the results obtained using noise statistics with state-of-the-art laser stabilization ( $\delta I \sim 0.007$ ,  $\Delta\phi = 0.01\pi$ ) [31] and sideband cooling ( $T = 3\mu\text{K}$ ), which show that errors in fidelity could, in principle, be reduced to less than 1%. In fact, all the errors in such conditions depend on  $\delta I$ , as practically the same results would be obtained at  $T = 30\mu\text{K}$ .

For implementations of the gate based on a single broad Gaussian beam [only valid in general for two qubits and positive  $x$  as in Fig. 1(c)],  $\delta x_k$  only depends on the thermal motion of the atoms to a good approximation, so the overall error is smaller. In Fig. 9 we show the infidelity,  $\epsilon = 1 - \bar{F}$ , of different gates with  $l'' = 0$  and increasing values of  $l'$  (correlated to increasing values of  $A^{\text{op}}$  and decreasing values of  $x^{\text{op}}$ ), prepared with a single-pulse protocol, implemented by a single beam or a superposition of two Gaussian beams, with different levels of noise. As observed, the results only differ for protocols with large  $l'$ .

On the other hand, because the error is dominated by fluctuations in the largest Rabi frequency, protocols that share the total area between two or more pulses will improve the average fidelity. In Fig. 9 we also show the gate infidelities for protocols based on two-pulse sequences (implemented by superposed Gaussian beams), using aligned structural vectors  $x_1 = x_2$ , in two cases: when  $A_1 = 7\pi$  and when  $A_1 = 14\pi$ . In these cases, from Eq. (11),  $A_T = A_2^{\text{op}} + A_1 = 4n + 2$  practically coincides with the previously optimized areas for single-pulse protocols. Therefore, to avoid double labels and to compare the fidelities obtained with protocols with the same

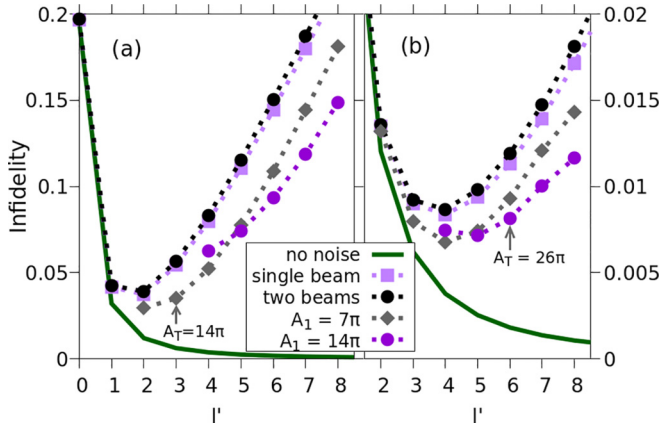


FIG. 9. Gate infidelity,  $1 - \bar{F}$ , in protocols corresponding to different  $l'$  numbers, for different implementations using a single Gaussian beam, two superposed Gaussian beams, and two-pulse sequences using superposed Gaussian beams with aligned structural vectors ( $x_1 = x_2$ ), where two possible values of  $A_1$  have been chosen. For the two-pulse sequence,  $l'$  corresponds to  $n$  in Eq. (11). In (a) we use standard noise statistics, while in (b) we use conditions labeled as ultra.

total area  $A_T$ , we also use  $l'$  instead of  $n$  for the two-pulse protocols in Fig. 9.

When  $A_1 = 7\pi$ , the error will be dominated by this pulse area until  $A_2$  is of the order or larger than  $7\pi$ . It is as if we had subtracted area from  $A_T$  so that the infidelities are shifted toward higher  $n$ . Hence, the error does not increase significantly until  $n > 3$  ( $A_T > 14\pi$ ). One can approximately control how to displace the error curves to larger  $n$  by choosing  $A_1$ . For instance, comparing the results for  $A_1 = 7\pi$  and  $A_1 = 14\pi$ , we observe the shifting toward higher  $n$  of the latter curve. If  $A_1 = 14\pi$ , the noise is approximately distributed equally among the pulses at  $A_2 = 12\pi$  ( $A_T = 26\pi$ ), so that the error will not significantly increase until  $n > 6$  ( $A_T > 26\pi$ ). This can be observed in the results with noise statistics corresponding to ultra conditions. In principle, one could extend this strategy to longer pulse sequences, using as many pulses as needed to adjust the largest pulse area allowed given the noise statistics of the setup, such that the infidelity is as small as possible.

## VI. CONCLUSIONS

By implementing qubits in atoms trapped at a short distance from each other, thereby boosting the dipole blockade, it is in principle possible to speed up the gates to the nanosecond timescale [61]. In this work, we have studied minimal pulse sequences that implement the CZ gate on two adjacent and

nonindependent qubits with high fidelity, where the number of pulses used per qubit can be as small as one. Indeed, using structured light, one can in principle implement the gate with a single pulse. We have proposed a possible implementation using superposed Gaussian beams, and we have analyzed the role of parameter fluctuations induced by shot-to-shot noise.

The optimal parameters must be approximate solutions of Diophantine equations, imposing strict conditions on the areas and overlaps between the pulses. While perfect fidelities can never be achieved even under ideal conditions, the errors can be made as small as desired using intense pulses. But, increasing the areas ultimately penalizes the minimum duration of the protocol, partially compensating the gains of using nonindependent qubits. Adopting two-pulse sequences alleviates restrictions on parameter values for optimizing the gate, allowing to lower the largest pulse areas. One finds that a continuum of mechanisms, described in terms of quantum pathways, can be used for its implementation, although strong correlations in the areas of the pulses of the form  $A_1 = (4l + 2)\pi$ ,  $A_2 = 4m\pi$  ( $l, m \in \mathbb{Z}$ ) or vice versa, are typically found in optimal protocols.

Analyzing the effect of noise on the fidelity of the proposed protocols, we found that intensity fluctuations have a much stronger impact on the gates than the thermal motion of the atoms, mainly in protocols with large pulse areas and, consequently, stronger fields (assuming that we use the shortest possible pulses). Our preliminary analysis reveals that the stabilization of the lasers that allows to reduce the relative errors in the pulse intensities below 1% may be necessary for the laboratory implementations of these protocols. On the other hand, the experiments could be performed at typical ultracold temperatures of  $\sim 100 \mu\text{K}$ .

While an in-depth analysis of all protocols can only be made for small pulse sequences, comparing the fidelities based on single pulses versus two-pulse sequences, we expect that the use of protocols with several pulses with similar total accumulated Rabi frequency, but smaller peak intensities, can result in higher fidelities and more robust gates.

## ACKNOWLEDGMENTS

This research was supported by the Quantum Computing Technology Development Program (Grant No. NRF-2020M3E4A1079793). I.R.S. thanks the BK21 program (Global Visiting Fellow) for the stay during which this project started and the Ministerio de Ciencia e Innovación of Spain (MICINN), Grant No. PID2021-122796NB-I00. B.Y.C. and S.S. acknowledge support from the Center for Electron Transfer funded by the Korean government (MSIT) (Grant No. NRF-2021R1A5A1030054).

- [1] N. P. de Leon, K. M. Itoh, D. Kim, K. K. Mehta, T. E. Northup, H. Paik, B. S. Palmer, N. Samarth, S. Sangtawesin, and D. W. Steuerman, Materials challenges and opportunities for quantum computing hardware, *Science* **372**, eabb2823 (2021).
- [2] S. G. J. Philips, M. T. Mądzik, S. V. Amitonov, S. L. de Snoo, M. Russ, N. Kalhor, C. Volk, W. I. L. Lawrie, D.

Brousse, L. Tryputen, B. P. Wuetz, A. Sammak, M. Veldhorst, G. Scappucci, and L. M. K. Vandersypen, Universal control of a six-qubit quantum processor in silicon, *Nature (London)* **609**, 919 (2022).

- [3] Y. Wu *et al.*, Strong quantum computational advantage using a superconducting quantum processor, *Phys. Rev. Lett.* **127**, 180501 (2021).

- [4] K. Wright *et al.*, Benchmarking an 11-qubit quantum computer, *Nat. Commun.* **10**, 5464 (2019).
- [5] O. V. Borzenkova, G. I. Struchalin, A. S. Kardashin, V. V. Krasnikov, N. N. Skryabin, S. S. Straupe, S. P. Kulik, and J. D. Biamonte, Variational simulation of Schwinger's Hamiltonian with polarization qubits, *Appl. Phys. Lett.* **118**, 144002 (2021).
- [6] T. M. Graham *et al.*, Multi-qubit entanglement and algorithms on a neutral-atom quantum computer, *Nature (London)* **604**, 457 (2022).
- [7] J. I. Cirac and P. Zoller, A scalable quantum computer with ions in an array of microtraps, *Nature (London)* **404**, 579 (2000).
- [8] T. D. Ladd, F. Jelezko, R. Laflamme, Y. Nakamura, C. Monroe, and J. L. O'Brien, Quantum computers, *Nature (London)* **464**, 45 (2010).
- [9] M. H. Devoret and R. J. Schoelkopf, Superconducting circuits for quantum information: An outlook, *Science* **339**, 1169 (2013).
- [10] J. Kelly *et al.*, State preservation by repetitive error detection in a superconducting quantum circuit, *Nature (London)* **519**, 66 (2015).
- [11] T. P. Harty, D. T. C. Allcock, C. J. Ballance, L. Guidoni, H. A. Janacek, N. M. Linke, D. N. Stacey, and D. M. Lucas, High-fidelity preparation, gates, memory, and readout of a trapped-ion quantum bit, *Phys. Rev. Lett.* **113**, 220501 (2014).
- [12] F. Jelezko, T. Gaebel, I. Popa, M. Domhan, A. Gruber, and J. Wrachtrup, Observation of coherent oscillation of a single nuclear spin and realization of a two-qubit conditional quantum gate, *Phys. Rev. Lett.* **93**, 130501 (2004).
- [13] M. Saffman, T. G. Walker, and K. Mølmer, Quantum information with Rydberg atoms, *Rev. Mod. Phys.* **82**, 2313 (2010).
- [14] F. Nogrette, H. Labuhn, S. Ravets, D. Barredo, L. Béguin, A. Vernier, T. Lahaye, and A. Browaeys, Single-atom trapping in holographic 2D arrays of microtraps with arbitrary geometries, *Phys. Rev. X* **4**, 021034 (2014).
- [15] D. Barredo, S. de Léséleuc, V. Lienhard, T. Lahaye, and A. Browaeys, An atom-by-atom assembler of defect-free arbitrary two-dimensional atomic arrays, *Science* **354**, 1021 (2016).
- [16] J. T. Wilson, S. Saskin, Y. Meng, S. Ma, R. Dilip, A. P. Burgers, and J. D. Thompson, Trapping alkaline earth Rydberg atoms optical tweezer arrays, *Phys. Rev. Lett.* **128**, 033201 (2022).
- [17] A. P. Burgers, S. Ma, S. Saskin, J. Wilson, M. A. Alarcón, C. H. Greene, and J. D. Thompson, Controlling Rydberg excitations using ion-core transitions in alkaline-earth atom-tweezer arrays, *PRX Quantum* **3**, 020326 (2022).
- [18] W. Lee, H. Kim, and J. Ahn, Three-dimensional rearrangement of single atoms using actively controlled optical microtraps, *Opt. Express* **24**, 9816 (2016).
- [19] D. Comparat and P. Pillet, Dipole blockade in a cold Rydberg atomic sample, *J. Opt. Soc. Am. B* **27**, A208 (2010).
- [20] D. Tong, S. M. Farooqi, J. Stanojevic, S. Krishnan, Y. P. Zhang, R. Côté, E. E. Eyler, and P. L. Gould, Local blockade of Rydberg excitation in an ultracold gas, *Phys. Rev. Lett.* **93**, 063001 (2004).
- [21] E. Urban, T. A. Johnson, T. Henage, L. Isenhower, D. D. Yavuz, T. G. Walker, and M. Saffman, Observation of Rydberg blockade between two atoms, *Nat. Phys.* **5**, 110 (2009).
- [22] A. Gaëtan, Y. Miroshnychenko, T. Wilk, A. Chotia, M. Viteau, D. Comparat, P. Pillet, A. Browaeys, and P. Grangier, Observation of collective excitation of two individual atoms in the Rydberg blockade regime, *Nat. Phys.* **5**, 115 (2009).
- [23] J. D. Pritchard, D. Maxwell, A. Gauguier, K. J. Weatherill, M. P. A. Jones, and C. S. Adams, Cooperative atom-light interaction in a blockaded Rydberg ensemble, *Phys. Rev. Lett.* **105**, 193603 (2010).
- [24] D. Barredo, V. Lienhard, S. de Léséleuc, T. Lahaye, and A. Browaeys, Synthetic three-dimensional atomic structures assembled atom by atom, *Nature (London)* **561**, 79 (2018).
- [25] Y. Mei, Y. Li, H. Nguyen, P. R. Berman, and A. Kuzmich, Trapped alkali-metal Rydberg qubit, *Phys. Rev. Lett.* **128**, 123601 (2022).
- [26] Y. O. Dudin and A. Kuzmich, Strongly interacting Rydberg excitations of a cold atomic gas, *Science* **336**, 887 (2012).
- [27] C. S. Adams, J. D. Pritchard, and J. P. Shaffer, Rydberg atom quantum technologies, *J. Phys. B: At. Mol. Opt. Phys.* **53**, 012002 (2019).
- [28] Y. Chew, T. Tomita, T. P. Mahesh, S. Sugawa, S. de Léséleuc, and K. Ohmori, Ultrafast energy exchange between two single Rydberg atoms on a nanosecond timescale, *Nat. Photonics* **16**, 724 (2022).
- [29] H. Levine, A. Keesling, A. Omran, H. Bernien, S. Schwartz, A. S. Zibrov, M. Endres, M. Greiner, V. Vuletić, and M. D. Lukin, High-fidelity control and entanglement of Rydberg-atom qubits, *Phys. Rev. Lett.* **121**, 123603 (2018).
- [30] Y. Zeng, P. Xu, X. He, Y. Liu, M. Liu, J. Wang, D. J. Papoular, G. V. Shlyapnikov, and M. Zhan, Entangling two individual atoms of different isotopes via Rydberg blockade, *Phys. Rev. Lett.* **119**, 160502 (2017).
- [31] H. Jo, Y. Song, M. Kim, and J. Ahn, Rydberg atom entanglements in the weak coupling regime, *Phys. Rev. Lett.* **124**, 033603 (2020).
- [32] T. Wilk, A. Gaëtan, C. Evellin, J. Wolters, Y. Miroshnychenko, P. Grangier, and A. Browaeys, Entanglement of two individual neutral atoms using Rydberg blockade, *Phys. Rev. Lett.* **104**, 010502 (2010).
- [33] K. M. Maller, M. T. Lichtman, T. Xia, Y. Sun, M. J. Piotrowicz, A. W. Carr, L. Isenhower, and M. Saffman, Rydberg-blockade controlled-not gate and entanglement in a two-dimensional array of neutral-atom qubits, *Phys. Rev. A* **92**, 022336 (2015).
- [34] X. L. Zhang, L. Isenhower, A. T. Gill, T. G. Walker, and M. Saffman, Deterministic entanglement of two neutral atoms via Rydberg blockade, *Phys. Rev. A* **82**, 030306(R) (2010).
- [35] C. J. Picken, R. Legaie, K. McDonnell, and J. D. Pritchard, Entanglement of neutral-atom qubits with long ground-Rydberg coherence times, *Quantum Sci. Technol.* **4**, 015011 (2018).
- [36] V. S. Malinovsky and I. R. Sola, Quantum control of entanglement by phase manipulation of time-delayed pulse sequences. I, *Phys. Rev. A* **70**, 042304 (2004).
- [37] V. S. Malinovsky and I. R. Sola, Quantum phase control of entanglement, *Phys. Rev. Lett.* **93**, 190502 (2004).
- [38] V. S. Malinovsky and I. R. Sola, Phase-controlled collapse and revival of entanglement of two interacting qubits, *Phys. Rev. Lett.* **96**, 050502 (2006).
- [39] D. Jaksch, J. I. Cirac, P. Zoller, S. L. Rolston, R. Côté, and M. D. Lukin, Fast quantum gates for neutral atoms, *Phys. Rev. Lett.* **85**, 2208 (2000).
- [40] L. Isenhower, M. Saffman, and K. Mølmer, Multibit CkNOT quantum gates via Rydberg blockade, *Quant. Info. Proc.* **10**, 755 (2011).
- [41] M. D. Lukin, M. Fleischhauer, R. Cote, L. M. Duan, D. Jaksch, J. I. Cirac, and P. Zoller, Dipole blockade and quantum

- information processing in mesoscopic atomic ensembles, *Phys. Rev. Lett.* **87**, 037901 (2001).
- [42] H. Levine, A. Keesling, G. Semeghini, A. Omran, T. T. Wang, S. Ebadi, H. Bernien, M. Greiner, V. Vuletić, H. Pichler, and M. D. Lukin, Parallel implementation of high-fidelity multiqubit gates with neutral atoms, *Phys. Rev. Lett.* **123**, 170503 (2019).
- [43] S. R. Cohen and J. D. Thompson, Quantum computing with circular Rydberg atoms, *PRX Quantum* **2**, 030322 (2021).
- [44] X.-F. Shi, Quantum logic and entanglement by neutral Rydberg atoms: Methods and fidelity, *Quantum Sci. Technol.* **7**, 023002 (2022).
- [45] X.-F. Shi, Deutsch, Toffoli, and CNOT gates via Rydberg blockade of neutral atoms, *Phys. Rev. Appl.* **9**, 051001(R) (2018).
- [46] D. Paredes-Barato and C. S. Adams, All-optical quantum information processing using Rydberg gates, *Phys. Rev. Lett.* **112**, 040501 (2014).
- [47] V. S. Malinovsky, I. R. Sola, and J. Vala, Phase-controlled two-qubit quantum gates, *Phys. Rev. A* **89**, 032301 (2014).
- [48] M. H. Goerz, T. Calarco, and C. P. Koch, The quantum speed limit of optimal controlled phasegates for trapped neutral atoms, *J. Phys. B: At. Mol. Opt. Phys.* **44**, 154011 (2011).
- [49] M. Morgado and S. Whitlock, Quantum simulation and computing with Rydberg-interacting qubits, *AVS Quantum Sci.* **3**, 023501 (2021).
- [50] J. T. Young, P. Bienias, R. Belyansky, A. M. Kaufman, and A. V. Gorshkov, Asymmetric blockade and multiqubit gates via dipole-dipole interactions, *Phys. Rev. Lett.* **127**, 120501 (2021).
- [51] M. Saffman, I. I. Beterov, A. Dalal, E. J. Pérez, and B. C. Sanders, Symmetric Rydberg controlled- $z$  gates with adiabatic pulses, *Phys. Rev. A* **101**, 062309 (2020).
- [52] C. Zhang, F. Pokorny, W. Li, G. Higgins, A. Pöschl, I. Lesanovsky, and M. Hennrich, Submicrosecond entangling gate between trapped ions via Rydberg interaction, *Nature (London)* **580**, 345 (2020).
- [53] M. Khazali and K. Mølmer, Fast multiqubit gates by adiabatic evolution in interacting excited-state manifolds of Rydberg atoms and superconducting circuits, *Phys. Rev. X* **10**, 021054 (2020).
- [54] M. Khazali, All-optical quantum information processing via a single-step Rydberg blockade gate, *Opt. Express* **31**, 13970 (2023).
- [55] L. Zhang, V. Walther, K. Mølmer, and T. Pohl, Photon-photon interactions in Rydberg-atom arrays, *Quantum* **6**, 674 (2022).
- [56] S. E. Anderson, K. C. Younge, and G. Raithel, Trapping Rydberg atoms in an optical lattice, *Phys. Rev. Lett.* **107**, 263001 (2011).
- [57] E. Crane, A. Schuckert, N. H. Le, and A. J. Fisher, Rydberg entangling gates in silicon, *Phys. Rev. Res.* **3**, 033086 (2021).
- [58] Y. Song, M. Kim, H. Hwang, W. Lee, and J. Ahn, Quantum simulation of Cayley-tree Ising Hamiltonians with three-dimensional Rydberg atoms, *Phys. Rev. Res.* **3**, 013286 (2021).
- [59] M. Kim, Y. Song, J. Kim, and J. Ahn, Quantum Ising Hamiltonian programming in trio, quartet, and sextet qubit systems, *PRX Quantum* **1**, 020323 (2020).
- [60] M. H. Goerz, E. J. Halperin, J. M. Aytac, C. P. Koch, and K. B. Whaley, Robustness of high-fidelity Rydberg gates with single-site addressability, *Phys. Rev. A* **90**, 032329 (2014).
- [61] I. R. Sola, V. S. Malinovsky, J. Ahn, S. Shin, and B. Y. Chang, Two-qubit atomic gates: Spatio-temporal control of Rydberg interaction, *Nanoscale* **15**, 4325 (2023).
- [62] I. R. Sola, S. Shin, and B. Y. Chang, Finding, mapping, and classifying optimal protocols for two-qubit entangling gates, *Phys. Rev. A* **108**, 032620 (2023).
- [63] I. R. Sola, S. Shin, and B. Y. Chang, Optimal protocols for entangling gates in  $N$ -qubit atomic systems, *AIP Adv.* **13**, 115102 (2023).
- [64] N. Šibalić and C. S. Adams, *Rydberg Physics* (IOP Publishing, Bristol, 2018), pp. 2399–2891.
- [65] The scheme works similarly with pulses in resonance from the  $|1\rangle$  state to the Rydberg state.
- [66] M. V. R. K. Murty, A simple way of demonstrating the phase reversals in the  $TEM_{10}$ ,  $TEM_{20}$ ,  $TEM_{30}$  modes of a gas laser source, *Appl. Opt.* **3**, 1192 (1964).
- [67] A. Forbes, M. de Oliveira, and M. R. Dennis, Structured light, *Nat. Photonics* **15**, 253 (2021).
- [68] H. Rubinsztein-Dunlop *et al.*, Roadmap on structured light, *J. Opt.* **19**, 013001 (2017).
- [69] A. N. K. Reddy, S. Mahler, A. Goldring, V. Pal, A. A. Friesem, and N. Davidson, Phase locking of lasers with Gaussian coupling, *Opt. Express* **30**, 1114 (2022).
- [70] X. Chen, Y. Bai, M. Jiang, L. Li, Y. Zhou, H. Wang, Z. Ren, and J. Bai, Formation of four phase-locked gaussian beams by saturable absorber in a neodymium-doped yttrium aluminum garnet laser, *Appl. Phys. Express* **5**, 122701 (2012).
- [71] In spite of the fact that one can find protocols that maximize the fidelity for any type of mechanism, using optimal control algorithms in Ref. [62] we only found protocols for which the  $V$  subsystem is a zero-loop. An intriguing question is why this is so. We believe that the reason is rooted in the peak fidelities that can be achieved by the different mechanisms under moderate pulse areas. Because the fidelity of protocols based on aligned structural vectors behaves as in single-pulse protocols, one needs  $A_T \geq 14\pi$  (for  $l' = l, l'' = 0$ ) to achieve  $F \geq 0.99$ , while  $A_T \geq 38\pi$  (for  $l' = l, l'' = 0$ ) to achieve  $F \geq 0.999$ , which was the threshold chosen in Ref. [62] to analyze the chosen optimal protocols. Numerically, one finds many protocols with higher fidelity and lower pulse areas when the pulse areas are correlated as  $A_1 = (4l + 2)\pi$  and  $A_2 = 4m\pi$  or vice versa, imposing a zero-loop in the  $V$  subsystem. Only when one analyzes the set of optimal protocols with lower fidelities does one observe protocols with mechanisms that do not use the zero-loop for the  $V$  subsystem.
- [72] W. Lee, M. Kim, H. Jo, Y. Song, and J. Ahn, Coherent and dissipative dynamics of entangled few-body systems of Rydberg atoms, *Phys. Rev. A* **99**, 043404 (2019).
- [73] R. W. Williams, S. Schlücker, and B. S. Hudson, Inelastic neutron scattering, Raman, vibrational analysis with anharmonic corrections, and scaled quantum mechanical force field for polycrystalline L-alanine, *Chem. Phys.* **343**, 1 (2008).
- [74] R. Marquardt, Mean square displacement of a free quantum particle in a thermal state, *Mol. Phys.* **119**, e1971315 (2021).